Testing chameleon dark energy at short range with atom interferometer

Le-Le Chen, Wen-Jie Xu,* Min-Kang Zhou, and Zhong-Kun Hu
MOE Key Laboratory of Fundamental Physical Quantities Measurements, Hubei key Laboratory of Gravitation and Quantum Physics, PGMF and School of Physics, Huazhong University of Science and Technology, Wuhan 430074, China

(Received 17 March 2024; accepted 13 May 2024; published 7 June 2024)

We propose a method to constrain the chameleon dark energy using atom interference in an optical lattice by measuring the acceleration near a glass disk. Since the lattice fixes the positions of the atoms, our method is effective in suppressing the decay of the chameleon field with distance compared to the reported works with free-falling atoms. In addition, we choose a circular glass disk as the source mass, which makes the gravitational effect at close range almost invariant. The fixed atomic position and the symmetry of the source mass reduce the difficulty of studying the systematic errors. At the same acceleration measurement precision, our method is expected to have a larger chameleon parameter exclusion region than the atomic test for usual distances.

DOI: 10.1103/PhysRevD.109.123515

I. INTRODUCTION

Astronomical observations have proved that the Universe is expanding at an accelerating rate [1,2], and its cause remains one of the central questions of physics. Dark energy scalar field theories with the screening mechanisms [3–6] attempt to explain this phenomenon, which typically establish a physical field that is hidden from experimental detection when in regions of high matter density and exhibits long-range effects in low-density environments. Although these theories still have major flaws, such as the inability to explain the cosmological constant problem, experimental tests of them could inspire more convincing explanations in the future.

The most representative dark energy scalar field models include the chameleon [3,7] and the symmetron [8,9]. A number of methods have been developed by various research groups for the detection of chameleon scalar field. These methods include the torsion balance experiments [10,11], the microsphere force sensing [12], the neutron experiments [13,14], and the levitated force sensor [15]. In addition to direct tests of the chameleon, there are test experiments based on the assumption that there is additional coupling between the photon and the chameleon. These include the Chameleon Afterglow Search experiment [16,17], the Axion Dark Matter Experiment (ADMX) [18], and the tests based on astronomical observations [19–21]. In contrast to these works, experiments based on dilute gas atoms in a vacuum effectively avoid the screening effect of the detector itself on the chameleon field, thus making a breakthrough in constrains on chameleon parameters.

Since the first proposal to test the chameleon field with atoms in a vacuum chamber [22], a number of light-pulsed atom interferometers based on the use of free-falling atoms have been performed to achieve constraints on the chameleon parameters [23–25]. In these works, the chameleon parameter exclusion region is closely related to the measurement of source mass-induced chameleon acceleration. However, similar to the gravitational field, the chameleon field exhibits a decay with distance. As a result, the free fall of the atoms would limit the interrogation time of the atom interferometer, preventing the interferometer from achieving optimal sensitivity. In addition, the systematic effects are difficult to evaluate because the distance between the test atom and the source mass changes with the fall time.

A number of ambitious projects have been proposed pursue higher levels of chameleon testing, e.g., through the use of the multiring atomic interferometer (MRA) and the multiplying source mass [26,27]. These programs will significantly improve the possible signals of chameleon test experiments and are expected to greatly expand the chameleon parameter exclusion region. From another independent line of thought, we propose the use of a circular planar glass disk as a source mass and the fixing of atoms in an optical lattice for short-range testing to obtain a stronger signal. This application coincides with the intended application of optical lattice atom interferometry [28–32]. As atoms are held by the optical lattice, signal attenuation of the chameleon field due to falling is avoided. In addition, this scheme has an advantage over falling atoms in terms of systematic error modeling, since the falling trajectories of atoms do not need to be taken into account anymore.

*wenjiexu@hust.edu.cn

The paper is organized as follows: in Sec. II, we present the form of the source mass-induced chameleon; in Sec. III, we show the design of the experimental configuration of the interferometry experiment for measuring the acceleration of the chameleon. In Sec. IV, we discuss the main systematic error effects. Section V gives the expected chameleon parameter exclusion region. Finally, we summarize this work in Sec. VI and acknowledgements in the last section.

II. GRAVITY AND CHAMELEON FIELD NEAR THE DISK

The source mass plays a crucial role in chameleon dark energy test experiments. Reported works on source mass design has shown that the chameleon acceleration exhibits a rapid decay with distance for both spherical and cylindrical source masses [33]. We are inspired by this and propose a method to test the chameleon field near the surface of a glass disk. Our analysis reveals excellent properties of both the gravity field and the chameleon field around the circular glass disk.

For the gravity field, when the test point is near the center of a thin disk, the gravity is similar to the one near the infinity plane, which produces an almost constant gravitational acceleration. The configuration of the atom and disk is designed as shown in Fig. 1. We selected the coordinate axes so that the disk is just in the $z \leq 0$ region and the disk's axis of symmetry coincides with the z axis. Integrating the gravity induced by each part of the disk at a specific point on the z-axis gives the magnitude of the gravitational acceleration induced by the source mass, which is

$$a_G = -2\pi G\rho_m\left(d + \sqrt{R^2 + z^2} - \sqrt{R^2 + (d+z)^2}\right), \quad (1)$$

where z is the distance between the surface of the disk and the test point, and d, ρ_m, R are the thickness, density and radius of the glass disk, respectively.

The distribution of gravitational acceleration is shown in Fig. 2, and for the parameters we consider, i.e., $z \leq 1$ mm

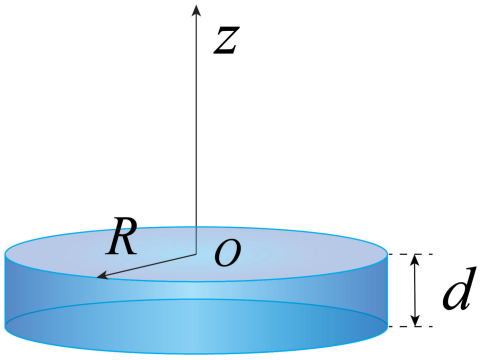

FIG. 1. The disc-shaped source mass and the coordinates.

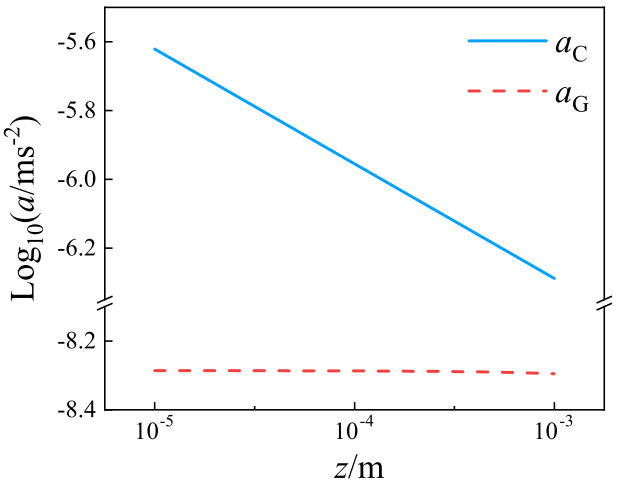

FIG. 2. The accelerations due to the gravity and the chameleon of the glass disc. The red dashed line shows the gravity acceleration a_G, and the blue solid line shows the chameleon acceleration a_C. The parameters of the glass disc and the chameleon field are $R = 50$ mm, $d = 5$ mm, $\rho = 2.6 \times 10^3$ kg/m^3, $\Lambda = 2.4$ meV, $\beta = 10^3$ and $n = 1$.

and $R = 50$ mm, the change in acceleration is only about 2% over the entire test range of z. This can also be explained by the approximation of Eq. 1 under the condition of $d, z \ll R$, which gives

$$a_G \approx -2\pi G\rho_m d\left(1 - \frac{1}{2}\frac{d}{R} - \frac{z}{R}\right). \quad (2)$$

This equation shows that the gravitational acceleration is almost constant in the vicinity of the disk plane, which can effectively suppress the variations in gravitational acceleration caused by positioning errors when performing experiments.

On the other hand, for the chameleon field in the neighborhood of the disk we can obtain its analytic expression [34,35]. In this work, we focus on the non-relativistic steady state chameleon field in the inverse power law form, which satisfies the Klein-Gordon equation

$$\nabla\phi = -\frac{\Lambda^{n+4}}{\phi^{n+1}} + \frac{\rho}{M}, \quad (3)$$

both inside and outside the disc. Here n is a real index usually taken to be 1, ρ is the local density of matter, Λ sets the self-interaction strength of the field, and M characterizes the coupling between the chameleon and the matter. In Eq. (3) we have chosen the natural units, where $c = \hbar = 1$. M and the Planck mass M_{Pl} differ by β, i.e., $M = M_{\mathrm{Pl}}/\beta$.

The field profile near the disc can be solves as [34]

$$\phi = \phi_0\left[1 + \frac{2+n}{\sqrt{2n(n+1)}}m_\phi z\right]^{2/(2+n)}, \quad (4)$$

where

$$m_\phi = \sqrt{n(n+1)\frac{\Lambda^{n+4}}{\phi_0^{n+2}}} \tag{5}$$

is the mass of the chameleon at the boundary, and

$$\phi_0 \approx \frac{1}{n}\left(n\frac{\Lambda^{n+4}M_{\rm Pl}}{\beta\rho_{\rm disc}}\right)^{1/(n+1)} \tag{6}$$

is the chameleon field at the boundary. Here, $\rho_{\rm disc}$ is the density of the disc, which is about 2.6×10^3 kg/m^3 for this work.

Within the test distance we designed, z ranges from 50 μm to 1 mm, at which point the relation $m_\phi z > 1$ is satisfied as long as $\beta > 4$. Therefore, for the parameter space of $\beta \gg 10$, the first term in the bracket of Eq. (4) can be ignored. At this point, Eq. (4) can be approximated as

$$\phi(z) \approx \Lambda\left(\frac{2+n}{\sqrt{2}}\Lambda z\right)^{2/(2+n)}. \tag{7}$$

That is, when the coupling strength β is large enough, the chameleon field near the disk depends only on Λ and n.

The acceleration produced by the chameleon interaction on the test particle can be deduced from

$$a_C = \frac{1}{M}\eta\nabla\phi, \tag{8}$$

where $0 \le \eta \le 1$ is a screening function that depends on the mass and radius of the test particle, as well as the background value of the chameleon field in the vacuum cavity. Within the parameter space we are interested in, we roughly assume that $\eta \to 1$ holds for the test atoms considered in this work. Applying Eq. (8) to the field represented by the substitution of Eq. (7) yields

$$a_C = \frac{\beta}{M_{\rm Pl}}\Lambda 2^{1/(n+2)}\left(\frac{2+n}{2}\frac{z}{\lambda_C}\right)^{-n/(n+2)}\frac{1}{\lambda_C}, \tag{9}$$

where $\lambda_C = 1/\Lambda$ is the characteristic length of the chameleon, and λ_C is about 82 μm when $\Lambda = \Lambda_0 \approx 2.4$ meV, which corresponds to the parameters that make chameleon theory compatible with cosmic observations. The chameleon acceleration a_C versus the test distance z is also shown in Fig. 2. The chameleon-related information can be obtained by measuring the acceleration at different distances excluding the effect of invariant gravity.

III. ACCELERATION MEASUREMENT SCHEME

The experimental setup we designed is shown in Fig. 3, in which a glass disc is placed in the center of a vacuum cavity to generate the chameleon field. Cold atoms trapped by an optical dipole trap are loaded into an optical lattice and then transported to the vicinity of the glass disc via an optical elevator [36]. We use an interferometer method similar to that of the LNE-SYRTE in France [30,37,38] to measure the acceleration. This method allows close measurements of acceleration at high spatial resolution.

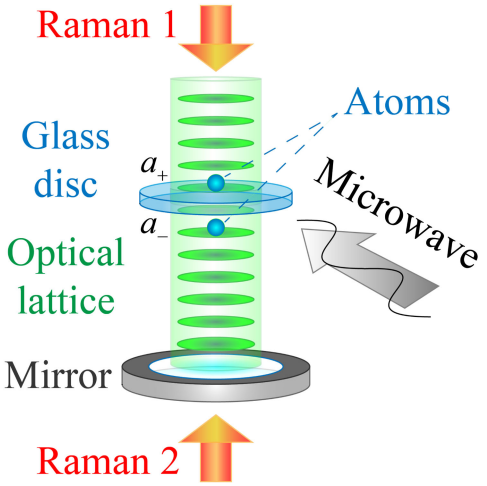

FIG. 3. Experimental setup for measuring the acceleration of a chameleon. In this case, a glass disk is used to generate the chameleon field, and each cloud of atoms above and below it is used as a test mass. The accelerations above and below the glass disk are a_+ and a_-, respectively. The optical lattice provides the potential well that maintains the position of the atoms constant. The Raman beams and the microwave are used for atomic interference.

Before the acceleration is measured experimentally, the position of the atom cloud from the surface of the glass disc needs to be precisely located. In our design, the atoms are loaded into a fixed position by an optical dipole trap during preparation, and then moved precisely to the desired position between the dipole trap and the glass disc surface by an optical lattice elevator. The elevator is then used to return the atoms to their original position for detection. During this process, the number of atoms is lost when the atoms kick into the glass surface, meaning that the distance between the glass surface and the dipole trap can be measured by the relationship between the distance the atoms are moved and the number of atoms remaining after the round trip. With this method [36,38], the distance between the atomic cloud center and the glass disc surface can be accurately controlled down to 0.1 μm [38].

Over a range of several lattice wavelengths, we can approximate the chameleon acceleration as a constant. Atoms in an optical lattice and within a constant acceleration field will form the ladder of Wannier-Stark states $|WS_j\rangle$, where j denotes the index that marks the lattice site. The constant spacing between two consecutive Wannier-Stark states can be given by the following relation

$$\hbar\omega_B = m_A a_\pm \lambda_L/2, \tag{10}$$

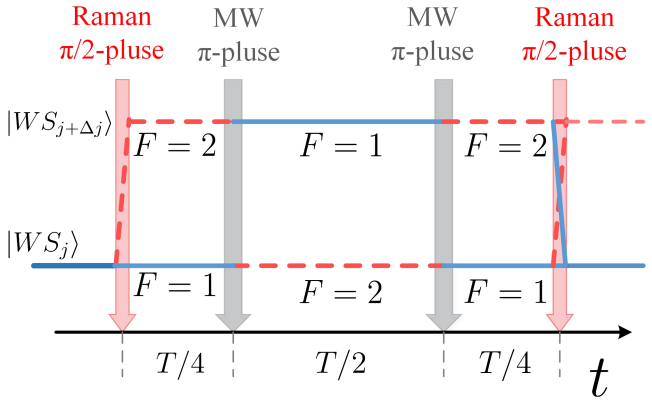

FIG. 4. Timing of Raman and microwave pulses used to manipulate the Wannier-Stark state of an atom for interference. In this process, the quantum number of the WS state of the atom transitions between j (lower line) and $j+\Delta j$ (upper line). The blue solid line in the figure indicates the $F=1$ state and the red dashed line indicates the $F=2$ state.

where $\hbar$ is the Planck's constant, ω_B is the angular frequency of the atomic Bloch oscillation, m_A is the mass of atom. The acceleration suffered by the upper and lower atom clouds shown in Fig. 3 can be expressed as

$$a_{\pm} = g_0(z) \pm (a_G + a_C), \tag{11}$$

which is the total acceleration due to local gravity $g_0(z)$, the Newtonian gravity of the disc a_G, and the chameleon field a_C. λ_L is the wavelength of the optical lattice.

We use a Ramsey-Raman interferometer shown in Fig. 4 to accurately measure the Bloch oscillation frequency of atoms. The atoms are first prepared into the ladder of Wannier-Stark states with $F=1$. In order to suppress the Zeeman shift, the atoms in this work are always in the $m_F=0$ sub-state. Then the atoms in the state $|F=1, WS_j\rangle$ are beam-split into the superposition states of $|F=1, WS_j\rangle$ and $|F=2, WS_{j+\Delta j}\rangle$ by a Raman $\pi/2$ pulse. After the evolution of T, the atoms are overlapped by a second Raman $\pi/2$ pulse. During the evolution, the internal state of each atom is inverted twice by two microwave π pulses spaced at $T/2$ intervals, thus suppressing the phase difference due to the evolution of the atomic internal state.

After the interference, the probability of the atomic state transition is

$$P = \frac{1}{2}[1-\cos(\Delta\varphi)], \tag{12}$$

where $\Delta\varphi$ is the phase difference accumulated by the upper and lower Wannier-Stark states, which is given by

$$\Delta\varphi = \Delta\varphi_{\mathrm{MW}} + \Delta\varphi_{\mathrm{Raman}} - \Delta j\omega_B T, \tag{13}$$

the sum of the phases due to the microwave $\Delta\varphi_{\mathrm{MW}}$, the Raman beams $\Delta\varphi_{\mathrm{Raman}}$, and the atomic acceleration $-\Delta j\omega_B T$.

The acceleration can be obtained from the fringes of a Ramsey-Raman interferometer. Specifically, the phases $\Delta\varphi_{\mathrm{MW}}$ and $\Delta\varphi_{\mathrm{Raman}}$ can be set by instruments, and the phase difference $\Delta\varphi$ between the two arms of the atomic interferometer can be varied by the phase of either the microwave or Raman beams. By changing the phase difference $\Delta\varphi = \varphi_0 + \delta\varphi$ and probing the atomic state transition probability P, we can obtain $\Delta\varphi$-P curves, i.e., the interference fringes. Thereafter the acceleration of the atom can be measured from the phase φ_0 obtained from the sinusoidal fit.

We obtain the signal of the possible chameleon field by differencing the atomic acceleration at different distances above and below the glass disk. According to Eq. 11, the difference between the accelerations above and below the glass disk is

$$\Delta a = a_+ - a_- = \gamma\Delta z + 2(a_G + a_C). \tag{14}$$

With this method it is possible to cancel out the average gravity, leaving only the gravity gradient effect $\gamma\Delta z$, where γ is the linear gravity gradient and Δz is the height difference between the upper and lower test points. Estimated according to our design parameters, the difference in acceleration between the upper and lower atoms due to the gravity gradient is about 1.8×10^{-8} m/s^2, which is discussed in detail in Section IV.

Because the Newtonian gravitational acceleration of the disk varies very little over the range of distances we tested, the Newtonian gravity signal a_G can be canceled out by differencing over different distances. For example, we estimate the acceleration at 50 μm and 1 mm respectively and then performed the difference. Assuming $\Lambda = 2.4$ meV, $n=1$, and $\beta=10^3$, the change in acceleration due to the chameleon field can be calculated from Eq. (9) to be $\Delta a_C = 8.8\times10^{-7}$ m/s^2. At the same time, the change in gravitational acceleration calculated from Eq. (1) is $\Delta a_G = 1.0\times10^{-10}$ m/s^2, a change of only about $\Delta a_G/a_G = 2\%$, much smaller than the possible differential signal of acceleration from the chameleon field.

IV. SYSTEMATIC ERROR EFFECTS

The Casimir Polder force is one of the most dominant effects affecting the results due to the close distance between the atoms and the surface of the glass disk. When the distance is greater than the thermal wavelength $\lambda_B = \hbar c/k_B T \approx 7.6$ μm, the asymptotic expression for the Casimir Polder acceleration can be written as [39]

$$a_{\mathrm{CPF}} = \frac{3\alpha_0 k_B T}{4mz^4}\frac{\epsilon_0 - 1}{\epsilon_0 + 1} \tag{15}$$

where α_0 is the static atomic polarizability, m is the atomic mass, and ϵ_0 is the dielectric constant of glass. A comparison of the Casimir Polder force effect with the

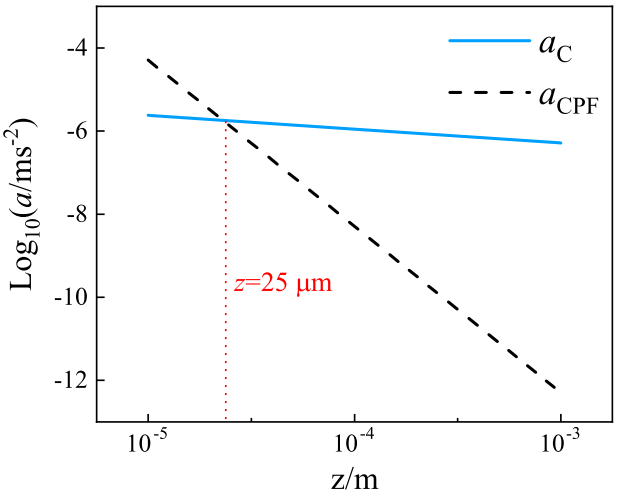

FIG. 5. Effect of Casimir Polder force with distance and possible chameleon acceleration. The Casimir Polder effect dominates at distances $z < 25$ μm. Since this effect is proportional to $1/z^4$, it is significantly attenuated at the test distance of 50 μm, which is about an order of magnitude smaller than the possible chameleon acceleration. The parameters in the calculation of the Casimir Polder force effect are chosen as $\alpha_0 = 4.7 \times 10^{-29}$ m^3 [40], $\epsilon_0 = 3.4$, $T = 300$ K.

chameleon field acceleration is shown in Fig. 5. The Casimir Polder force dominates in the range of test distances < 25 μm, so the test distances selected for our scheme is 50 μm.

On the other hand, an electromagnetic force will be generated at close range due to electrostatic interactions between atoms in the optical lattice and the electric dipoles of atoms accumulated on the surface of the glass disc surface. The mechanism of this effect has been rationalized in Ref. [41] and its magnitude is equal to

$$a_{\mathrm{elec}} = -\frac{\alpha_0}{2m}\frac{\mathrm{d}}{\mathrm{d}z}|\vec{E}|^2 \tag{16}$$

where $\vec{E}$ is the electric field formed by the dipole momentum of the surface adsorbed atoms as a whole. This effect has been studied under similar conditions in Ref. [38]. In that work, after a week of continuous operation without preventing atoms from kicking into the surface, about 10^{10} atoms accumulated on the test surface. These atoms are Gaussian distributed with a radius of 90 μm, the accompanying electromagnetic effect can produce an acceleration of about 10^{-3} m/s^2 at 50 μm from the surface. This shows that the electromagnetic effect caused by spurious particles accumulating on the surfaces is huge when a wrong experimental arrangement is executed.

To suppress the dipole electric field effect of surface atoms, the accumulation of rubidium atoms on the glass surface should be suppressed as much as possible in the chameleon dark energy test experiments. Therefore, we keep the glass disk away from the center of the MOT trap and the dipole trap, and use an optical lattice elevator to transport the atoms back after the interference is complete. Furthermore, the adsorption of atoms on the glass surface can be further suppressed by heating [41] or light-induced atom desorption [42] if necessary. Since the dipole electric field force formed by surface-adsorbed atoms is proportional to the number of atoms accumulated [41], and our design will greatly limit the rate of their accumulation, we expect this effect to be effectively suppressed.

In our experimental scheme, although the average gravity gradient is eliminated by differencing, the residual gravity gradient is still able to influence the result. Based on the vertical linear gravity gradient γ of the Earth of about 3000E (3×10^{-6}/s^2), and the spacing of the two atomic clouds above and below the glass disk $\Delta z \approx 6$ mm, the difference in gravitational acceleration is estimated to be 1.8×10^{-8} m/s^2, which is comparable to the magnitude of the gravitational force generated by the glass disk. In addition, the gravity gradient effect can be efficiently corrected by measurements of the Earth's local gravity gradient and the precise localization of atoms.

Generally speaking, the systematic error effects of atomic interference in optical lattices are simpler in form compared to free-falling atoms. The systematic errors associated with the atomic trajectories are suppressed due to the fixed positions of the atoms. In this case the external physical field contributes additional interferometer phase mainly by affecting the atomic energy difference ΔE between the two arms of the interferometer. When the external physical field is stable, the mathematical form of this contribution is simple and equal to $\Delta ET/\hbar$, which reduces the difficulty of evaluating the systematic error.

V. EXPECTED CONSTRAINTS ON CHAMELEON PARAMETERS

The current state-of-the-art experiments for atomic gravity acceleration measurements based on optical lattice already reached very high precision [37,43,44]. On this basis, we expect the statistical uncertainty of the acceleration to reach 10^{-7} m/s^2. In addition, based on previous studies of the major systematic errors in atom interferometry [45–47], we estimate the uncertainty to reach the level of 10^{-7} m/s^2 as well. For the chameleon test, we set the distance of the atoms from the surface of the glass disk to 50 μm, which is a compromise between signal amplitude and the systematic error effects.

According to the estimated uncertainty of the acceleration, we can use Eq. (9) to calculate the exclusion region for the chameleon parameters expected in this work. When we set the parameter $n = 1$, the experiment will test the parameter space shown in the blue region in Fig. 6. Compared to the non-short-range atomic interference test, our scheme is more advantageous when the acceleration measurement uncertainties are the same, and it is complementary to the torsion balance experiments.

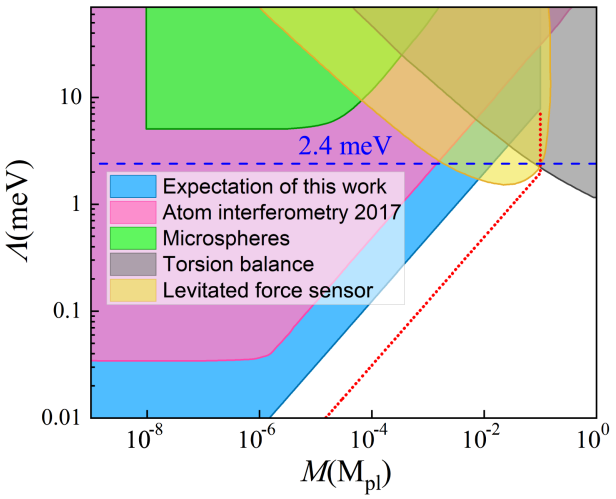

FIG. 6. Exclusion of chameleon parameters for $n = 1$. The blue dashed line corresponds to $\Lambda = \Lambda_0 \approx 2.4$ meV, which drives the cosmic acceleration today. Interferometer based on falling atoms in Ref. [24] excludes the pink region in the upper left. Region near the upper right with the gray color is excluded by the torsion balance [11]. The green area in the top left is the region where the microspheres are excluded [12]. The yellow color in the top center corresponds to the exclusion region given by the levitated force sensor [15]. The blue color in the figure shows the expected exclusion region for this work, which corresponds to an acceleration estimation uncertainty of 10^{-7} m/s^2. When the acceleration measurement level reaches 10^{-8} m/s^2, we expect the boundary of the exclusion region to be as shown by the red dotted line in the figure. Since our model applies to the case of $\beta \geq 10$, it leaves empty the exclusion region in the upper right where $M > 10^{-1} M_{\rm pl}$.

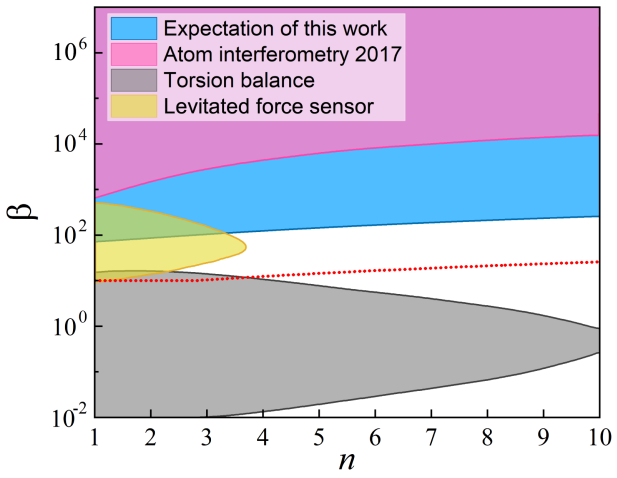

FIG. 7. Schematic diagram of the chameleon exclusion region in the n-β plane when $\Lambda = \Lambda_0$, where n is the power law index describing the shape of the chameleon potential. The excluded region for each experiment is labeled the same as in Fig. 5. In the estimation of the exclusion region, the distance of the test atoms from the glass disc is set to 50 μm. This distance is comparable to the length of the chameleon field feature length $\Lambda_C \approx 82$ μm. If acceleration measurements are made up to 10^{-8} m/s^2, the limits on β (shown by the red dotted line) will approach the precondition that Eq. (7) holds at our test distance.

On the basis of reported experiments with the atom interferometry [24], the torsion balance [11], and the levitation force sensor [15], the chameleon parameter exclusion space now overlaps around $\Lambda = \Lambda_0$, which almost completely rules out chameleon screened scalar field theory as a potential dark energy candidate. However, if this conclusion is scrutinized more critically, we will find that these experiments are based on different nuclear compositions and test qualities. These differences have the potential to disrupt the narrow overlap around $\Lambda =$ 2.4 meV in Fig. 6, which makes subsequent experimental work still important.

The blue region in Fig. 7 shows the region of exclusion that we expect in the n-β plane with $\Lambda = \Lambda_0$. This would place stronger constraints on the chameleon parameters than the reported works based on free-falling atoms [24,25]. The decay of the signal with n in Eq. (9) remains insignificant due to the similar size of our test distance z and the characteristic length of the chameleon λ_C. Thus the uncertainty of acceleration measurements limit β to roughly the same range under different chameleon field index factors n. This work will also compensate for the $n > 4$ region not tested by the levitated force sensor.

VI. CONCLUSION

The chameleon scalar field is a representative model of dark energy theory, and its testing is inspiring for dark energy research. This work shows that experiments using atoms in the optical lattice at short distances can effectively rule out the possible parameter regions of the chameleon. Acceleration measurements using an interferometer with atoms in the optical lattice are expected to improve the testing of dark energy with atom interferometry.

We use a glass disk as the source mass. In the close range, the acceleration produced by the chameleon and gravity, respectively, show different patterns of variation with distance. Since the variation of the gravitational acceleration with distance is almost zero in the range of $z \leq 1$ mm, differential measurements can suppress the gravitational effect even if the exact value of the gravitational constant G is not known, which will help to suppress the systematic error. Since the atomic positions are fixed, we also expect other systematic errors to have a simple form that is easy to evaluate.

Currently, our work is still only in the conceptual and preliminary design stage, and no experiments have been carried out yet. In the future, by modeling the chameleon field using a more accurate model rather than the approximate expression of Eq. 7, and by improving the acceleration measurements to the order of 10^{-8} m/s^2 or better, it will be possible to have a complete coverage of the chameleon field parameter exclusion region of $\Lambda = \Lambda_0$, $1 \leq n \leq 10$, $\beta \geq 1$ with our scheme. At the forefront of

research, pioneers are already working on testing dark energy with atoms in an optical lattice [44], and we expect this work to be of interest to related fields.

ACKNOWLEDGMENTS

We thank Zeng-li Li for his preliminary study on chameleon theory that inspired this work. This work is supported by the National Natural Science Foundation of China (Grants No. 12004128, No. 11727809, No. 11922404, No. 12104174, No. 12204186, No. 12274613), the National Key Research and Development Program of China (No. 2022YFC3003802, No. 2021YFB3900204), and the Department of Science and Technology of Hubei Province (No. 2022BAA018).

[1] N. Aghanim, Y. Akrami, M. Ashdown, J. Aumont, C. Baccigalupi, M. Ballardini, A. Banday, R. Barreiro, N. Bartolo *et al.* (Planck Collaboration), Planck 2018 results. VI. Cosmological parameters, Astron. Astrophys. **641**, A6 (2020).

[2] S. Perlmutter, G. Aldering, G. Goldhaber, R. Knop, P. Nugent, P. G. Castro, S. Deustua, S. Fabbro, A. Goobar, D. E. Groom *et al.*, Measurements of Ω and Λ from 42 high-redshift supernovae, Astrophys. J. **517**, 565 (1999).

[3] J. Khoury and A. Weltman, Chameleon fields: Awaiting surprises for tests of gravity in space, Phys. Rev. Lett. **93**, 171104 (2004).

[4] D. F. Mota and D. J. Shaw, Strongly coupled chameleon fields: New horizons in scalar field theory, Phys. Rev. Lett. **97**, 151102 (2006).

[5] K. Hinterbichler and J. Khoury, Screening long-range forces through local symmetry restoration, Phys. Rev. Lett. **104**, 231301 (2010).

[6] T. S. Koivisto, D. F. Mota, and M. Zumalacarregui, Screening modifications of gravity through disformally coupled fields, Phys. Rev. Lett. **109**, 241102 (2012).

[7] P. Brax, C. van de Bruck, A.-C. Davis, J. Khoury, and A. Weltman, Detecting dark energy in orbit: The cosmological chameleon, Phys. Rev. D **70**, 123518 (2004).

[8] K. A. Olive and M. Pospelov, Environmental dependence of masses and coupling constants, Phys. Rev. D **77**, 043524 (2008).

[9] K. Hinterbichler, J. Khoury, A. Levy, and A. Matas, Symmetron cosmology, Phys. Rev. D **84**, 103521 (2011).

[10] D. J. Kapner, T. S. Cook, E. G. Adelberger, J. H. Gundlach, B. R. Heckel, C. Hoyle, and H. E. Swanson, Tests of the gravitational inverse-square law below the dark-energy length scale, Phys. Rev. Lett. **98**, 021101 (2007).

[11] A. Upadhye, Dark energy fifth forces in torsion pendulum experiments, Phys. Rev. D **86**, 102003 (2012).

[12] A. D. Rider, D. C. Moore, C. P. Blakemore, M. Louis, M. Lu, and G. Gratta, Search for screened interactions associated with dark energy below the 100 μm length scale, Phys. Rev. Lett. **117**, 101101 (2016).

[13] T. Jenke, G. Cronenberg, J. Burgdörfer, L. Chizhova, P. Geltenbort, A. Ivanov, T. Lauer, T. Lins, S. Rotter, H. Saul *et al.*, Gravity resonance spectroscopy constrains dark energy and dark matter scenarios, Phys. Rev. Lett. **112**, 151105 (2014).

[14] K. Li, M. Arif, D. G. Cory, R. Haun, B. Heacock, M. G. Huber, J. Nsofini, D. A. Pushin, P. Saggu, D. Sarenac *et al.*, Neutron limit on the strongly-coupled chameleon field, Phys. Rev. D **93**, 062001 (2016).

[15] P. Yin, R. Li, C. Yin, X. Xu, X. Bian, H. Xie, C.-K. Duan, P. Huang, J.-h. He, and J. Du, Experiments with levitated force sensor challenge theories of dark energy, Nat. Phys. **18**, 1181 (2022).

[16] A. S. Chou, W. Wester, A. Baumbaugh, H. R. Gustafson, Y. Irizarry-Valle, P. Mazur, J. H. Steffen, R. Tomlin, A. Upadhye, A. Weltman *et al.*, Search for chameleon particles using a photon-regeneration technique, Phys. Rev. Lett. **102**, 030402 (2009).

[17] J. H. Steffen, A. Upadhye, A. Baumbaugh, A. S. Chou, P. O. Mazur, R. Tomlin, A. Weltman, and W. Wester, Laboratory constraints on chameleon dark energy and power-law fields, Phys. Rev. Lett. **105**, 261803 (2010).

[18] G. Rybka, M. Hotz, L. Rosenberg, S. Asztalos, G. Carosi, C. Hagmann, D. Kinion, K. van Bibber, J. Hoskins, C. Martin *et al.*, Search for chameleon scalar fields with the axion dark matter experiment, Phys. Rev. Lett. **105**, 051801 (2010).

[19] P. Brax and K. Zioutas, Solar chameleons, Phys. Rev. D **82**, 043007 (2010).

[20] C. Burrage, A.-C. Davis, and D. J. Shaw, Detecting chameleons: The astronomical polarization produced by chameleonlike scalar fields, Phys. Rev. D **79**, 044028 (2009).

[21] V. Anastassopoulos, S. Aune, K. Barth, A. Belov, H. Bräuninger, G. Cantatore, J. Carmona, J. Castel, S. Cetin, F. Christensen *et al.*, Improved search for solar chameleons with a gridpix detector at cast, J. Cosmol. Astropart. Phys. 01 (2019) 032.

[22] C. Burrage, E. J. Copeland, and E. Hinds, Probing dark energy with atom interferometry, J. Cosmol. Astropart. Phys. 03 (2015) 042.

[23] P. Hamilton, M. Jaffe, P. Haslinger, Q. Simmons, H. Müller, and J. Khoury, Atom-interferometry constraints on dark energy, Science **349**, 849 (2015).

[24] M. Jaffe, P. Haslinger, V. Xu, P. Hamilton, A. Upadhye, B. Elder, J. Khoury, and H. Müller, Testing sub-gravitational forces on atoms from a miniature in-vacuum source mass, Nat. Phys. **13**, 938 (2017).

[25] D. O. Sabulsky, I. Dutta, E. Hinds, B. Elder, C. Burrage, and E. J. Copeland, Experiment to detect dark energy forces using atom interferometry, Phys. Rev. Lett. **123**, 061102 (2019).

[26] S.-w. Chiow and N. Yu, Multiloop atom interferometer measurements of chameleon dark energy in microgravity, Phys. Rev. D **97**, 044043 (2018).
[27] F. Di Pumpo, A. Friedrich, and E. Giese, Optimal baseline exploitation in vertical dark-matter detectors based on atom interferometry, AVS Quantum Sci. **6**, 014404 (2024).
[28] P. Cladé, S. Guellati-Khélifa, C. Schwob, F. Nez, L. Julien, and F. Biraben, A promising method for the measurement of the local acceleration of gravity using bloch oscillations of ultracold atoms in a vertical standing wave, Europhys. Lett. **71**, 730 (2005).
[29] G. Ferrari, N. Poli, F. Sorrentino, and G. Tino, Long-lived Bloch oscillations with bosonic sr atoms and application to gravity measurement at the micrometer scale, Phys. Rev. Lett. **97**, 060402 (2006).
[30] Q. Beaufils, G. Tackmann, X. Wang, B. Pelle, S. Pelisson, P. Wolf, and F. P. Dos Santos, Laser controlled tunneling in a vertical optical lattice, Phys. Rev. Lett. **106**, 213002 (2011).
[31] B. Pelle, A. Hilico, G. Tackmann, Q. Beaufils, and F. P. Dos Santos, State-labeling Wannier-Stark atomic interferometers, Phys. Rev. A **87**, 023601 (2013).
[32] V. Xu, M. Jaffe, C. D. Panda, S. L. Kristensen, L. W. Clark, and H. Müller, Probing gravity by holding atoms for 20 seconds, Science **366**, 745 (2019).
[33] B. Elder, J. Khoury, P. Haslinger, M. Jaffe, H. Müller, and P. Hamilton, Chameleon dark energy and atom interferometry, Phys. Rev. D **94**, 044051 (2016).
[34] P. Brax and G. Pignol, Strongly coupled chameleons and the neutronic quantum bouncer, Phys. Rev. Lett. **107**, 111301 (2011).
[35] A. Ivanov, R. Höllwieser, T. Jenke, M. Wellenzohn, and H. Abele, Influence of the chameleon field potential on transition frequencies of gravitationally bound quantum states of ultracold neutrons, Phys. Rev. D **87**, 105013 (2013).
[36] F. Sorrentino, A. Alberti, G. Ferrari, V. Ivanov, N. Poli, M. Schioppo, and G. Tino, Quantum sensor for atom-surface interactions below 10 μm, Phys. Rev. A **79**, 013409 (2009).
[37] X. Alauze, A. Bonnin, C. Solaro, and F. P. Dos Santos, A trapped ultracold atom force sensor with a μm-scale spatial resolution, New J. Phys. **20**, 083014 (2018).
[38] Y. Balland, L. Absil, and F. P. d. Santos, Quectonewton local force sensor, arXiv:2310.14717.
[39] M. Antezza, L. P. Pitaevskii, and S. Stringari, New asymptotic behavior of the surface-atom force out of thermal equilibrium, Phys. Rev. Lett. **95**, 113202 (2005).
[40] M. Antezza, L. P. Pitaevskii, and S. Stringari, Effect of the casimir-polder force on the collective oscillations of a trapped Bose-Einstein condensate, Phys. Rev. A **70**, 053619 (2004).
[41] J. M. Obrecht, R. Wild, and E. A. Cornell, Measuring electric fields from surface contaminants with neutral atoms, Phys. Rev. A **75**, 062903 (2007).
[42] A. Gozzini, F. Mango, J. Xu, G. Alzetta, F. Maccarrone, and R. Bernheim, Light-induced ejection of alkali atoms in polysiloxane coated cells, Il Nuovo Cimento D **15**, 709 (1993).
[43] N. Poli, F.-Y. Wang, M. Tarallo, A. Alberti, M. Prevedelli, and G. Tino, Precision measurement of gravity with cold atoms in an optical lattice and comparison with a classical gravimeter, Phys. Rev. Lett. **106**, 038501 (2011).
[44] C. D. Panda, M. J. Tao, M. Ceja, and H. Müller, Measuring gravity by holding atoms, arXiv:2310.01344.
[45] A. Peters, K. Y. Chung, and S. Chu, High-precision gravity measurements using atom interferometry, Metrologia **38**, 25 (2001).
[46] M.-K. Zhou, Z.-K. Hu, X.-C. Duan, B.-L. Sun, J.-B. Zhao, and J. Luo, Precisely mapping the magnetic field gradient in vacuum with an atom interferometer, Phys. Rev. A **82**, 061602 (2010).
[47] A. Louchet-Chauvet, T. Farah, Q. Bodart, A. Clairon, A. Landragin, S. Merlet, and F. P. Dos Santos, The influence of transverse motion within an atomic gravimeter, New J. Phys. **13**, 065025 (2011).